Geometric properties and offset surface construction for slant timelike-ruled surfaces

Areej A. Almoneef
Department of Mathematical Sciences,
College of Sciences, Princess Nourah Bint Abdulrahman,
Riyadh 11546, KSA
Corresponding author: araalmoneef@gmail.com

Rashad A. Abdel-Baky
Department of Mathematics
Faculty of Science, University of Assiut,
71516 Assiut, Egypt
Corresponding author: rbaky@live.com

Abstract. This work investigates slant timelike-ruled surfaces and their evolute offsets in Minkowski 3-space $\mathbb{E}_1^3$. Using the symmetry of evolute curves, we derive a parametric formulation for skew timelike-ruled surfaces and establish conditions ensuring the coaxial alignment of the central normal with the ruling direction of the corresponding offset surface. The geometric properties are examined through the Blaschke and Darboux frames, leading to curvature characteristics and fundamental invariants. Special cases, such as timelike-developable and timelike-binormal surfaces, are analyzed with illustrative examples. These findings contribute to a deeper understanding of the differential geometry of timelike-ruled surfaces and their evolute offsets in Lorentzian space.

Key Words. Distribution parameter, Height functions, Osculating circle.
MSC (2020). 53A04, 53A05, 53A17.

1 Introduction

Ruled surfaces play a significant role in various fields such as design, architecture, manufacturing, sculpture, and art. They can be produced in a range of orientations, a topic that has been widely discussed in engineering and mathematical literature. In geometric representation, concepts are most effective when they are not too complex for engineers and practitioners to understand or too difficult to implement. These professionals apply mathematical models in practical scenarios, often in software environments like SolidWorks, AutoCAD, Rhinoceros 3D, and others. These tools are typically based on simple rational splines or polynomials, but more advanced mathematical models have yet to be fully implemented due to their complexity [1-7].

Parallel ruled surfaces, often referred to as offset ruled surfaces, are defined by the paths of lines that maintain a fixed distance from the original ruled surface along the normal direction. The study of these offset ruled surfaces in both

Euclidean and non-Euclidean 3-dimensional spaces is a fundamental area of research in geometry and physics. Over time, researchers have developed various results, theorems, and insights concerning these surfaces. In [8], the authors investigated the Bertrand offset for ruled surfaces and showed that, similarly to planar curves, a ruled surface can have an infinite number of Bertrand offsets. The relationship between the Bertrand offsets of trajectory ruled surfaces and their projections on spherical areas has been explored in [9, 10], along with their corresponding invariants. The Bertrand offsets of ruled surfaces in Minkowski 3-space were considered in [11, 12]. Additionally, the study of Mannheim offsets for timelike ruled and developable surfaces, particularly their invariants, was addressed in [13, 14]. In [15], Senturk and Yuce analyzed involute-evolute offsets of ruled surfaces and developed associated invariants using the geodesic Frenet frame. More recently, research on evolute offsets of ruled surfaces, especially those with constant Gaussian and mean curvatures, in both Euclidean and Minkowski 3-spaces has been presented in [16, 17].

The characteristics of ruled surfaces and their offset surfaces have been extensively studied in both Euclidean and non-Euclidean spaces (see [15-21]). However, existing literature lacks a detailed approach to constructing evolute offsets of slant $\mathfrak{TL}$-ruled surfaces in terms of the striction curve. In this study, we explore the geometric properties of slant $\mathfrak{TL}$-ruled surfaces and their evolute offsets within three-dimensional Minkowski space $\mathbb{E}_1^3$. By establishing a bijective correspondence through their rulings, we derive conditions under which an evolute offset $\mathfrak{M}^*$ maintains a coaxial relationship with the central normal of $\mathfrak{M}$. Furthermore, we formulate expressions governing curvature behavior and classify $\mathfrak{M}$ and $\mathfrak{M}^*$ based on specific functional parameters. Special cases, including $\mathfrak{TL}$-developable,$\mathfrak{TL}$-binormal, and $\mathfrak{TL}$-cone surfaces, are also examined, with graphical visualizations provided to support the analysis.

This paper investigates slant timelike ($\mathfrak{TL}$) ruled surfaces and their evolute offsets in Minkowski 3-space $\mathbb{E}_1^3$. We present a parametric formulation of skew $\mathfrak{TL}$-ruled surfaces and establish conditions ensuring the coaxial alignment of the central normal with the ruling direction of the corresponding offset surface. The study explores the geometric properties using the Blaschke and Darboux frames, deriving curvature characteristics and fundamental invariants. Special cases, including $\mathfrak{TL}$-developable and $\mathfrak{TL}$-binormal surfaces, are analyzed with illustrative examples. The findings provide a deeper understanding of the differential geometry of $\mathfrak{TL}$-ruled surfaces and their evolute offsets in Lorentzian space.

2   Basic concepts

Let $\mathbb{E}_1^3$ denote Minkowski 3-space [22, 23]. For vectors $\mathfrak{e} = (e_1, e_2, e_3)$ and $\nu = (\nu_1, \nu_2, \nu_3)$ in $\mathbb{E}_1^3$, the inner product is defined as:

$$< \mathfrak{e},\nu >= e_1\nu_1 + e_2\nu_2 - e_3\nu_3.$$

The cross product of $\mathfrak{e}$ and ν is given by:

$$\mathfrak{e} \times \nu = ((e_2\nu_3 - e_3\nu_2), (e_3\nu_1 - e_1\nu_3), -(e_1\nu_2 - e_2\nu_1)).$$

Since $< , >$ is an indefinite metric, a vector $\mathfrak{e} \in \mathcal{E}_1^3$ is classified as follows:
- Spacelike $(\mathfrak{S}\mathfrak{L})$ if $< \mathfrak{e}, \mathfrak{e} >> 0$ or $\mathfrak{e} = \mathbf{0}$,
- Timelike $(\mathfrak{T}\mathfrak{L})$ if $< \mathfrak{e}, \mathfrak{e} >< 0$,
- Lightlike or null if $< \mathfrak{e}, \mathfrak{e} >= 0$ and $\mathfrak{e} \neq \mathbf{0}$.

A curve γ in $\mathbb{E}_1^3$ is classified locally as $\mathfrak{S}\mathfrak{L}$, $\mathfrak{T}\mathfrak{L}$ or null (lightlike), if all of its tangent vectors γ' are $\mathfrak{S}\mathfrak{L}$, $\mathfrak{T}\mathfrak{L}$ or null (lightlike), respectively. The norm of a vector $\mathfrak{e} \in \mathcal{E}_1^3$ is defined as: $\|\mathfrak{e}\| = \sqrt{|< \mathfrak{e}, \mathfrak{e} >|}$. The unit spheres in hyperbolic and Lorentzian (de Sitter) space are:

$$\mathcal{H}_+^2 = \{\mathfrak{e} \in \mathbb{E}_1^3 \mid \|\mathfrak{e}\|^2 := e_1^2 + e_2^2 - e_3^2 = -1\}, \tag{1}$$

and

$$\mathcal{S}_1^2 = \{\mathfrak{e} \in \mathbb{E}_1^3 \mid \|\mathfrak{e}\|^2 := e_1^2 + e_2^2 - e_3^2 = 1\}. \tag{2}$$

3 Main results

In this section, we examine slant timelike-ruled surfaces and their evolute offsets in Minkowski 3-space $\mathbb{E}_1^3$. We established conditions ensuring coaxial alignment between the central normal of a slant $\mathfrak{T}\mathfrak{L}$-ruled surface $\mathfrak{M}$ and the ruling of its offset $\mathfrak{M}^*$. Curvature properties are derived, and classifications based on parameter choices are presented. Special cases, including $\mathfrak{T}\mathfrak{L}$-developable and $\mathfrak{T}\mathfrak{L}$-binormal surfaces, are analyzed with graphical illustrations.

A skew (non-developable) $\mathfrak{T}\mathfrak{L}$-ruled surface in $\mathbb{E}_1^3$ can be expressed using the parametric representation:

$$\mathfrak{M} : \boldsymbol{x}(v,t) = \boldsymbol{z}(v) + t\boldsymbol{k}(v), \ v \in I, \ t \in \mathbb{R}, \tag{3}$$

where $\boldsymbol{z}(v)$ is the striction curve, i.e., $< \boldsymbol{z}', \boldsymbol{k}' >= 0$, and v is the arc-length parameter of $\boldsymbol{k}(v) \in \mathcal{S}_1^2$, with

$$\|\boldsymbol{k}\|^2 = \left\|\boldsymbol{k}'\right\|^2 = 1, \ ('= \frac{d}{dv}).$$

This representation facilitates the kinematic-geometry analysis of $\mathfrak{M}$. The Blaschke frame for $\boldsymbol{k}(v) \in \mathcal{S}_1^2$ is given by

$$\left.\begin{array}{l} \boldsymbol{k} = \boldsymbol{k}_1(v), \ \boldsymbol{k}_2(v) = \boldsymbol{k}', \ \boldsymbol{k}_1 \times \boldsymbol{k}_2 = \boldsymbol{k}_3, \\ \boldsymbol{k}_1 \times \boldsymbol{k}_3 = \boldsymbol{k}_2, \ \boldsymbol{k}_2 \times \boldsymbol{k}_3 = -\boldsymbol{k}_1, \\ \|\boldsymbol{k}\|^2 = \left\|\boldsymbol{k}'\right\|^2 = -\|\boldsymbol{k}_3\|^2 = 1, \end{array}\right\} \tag{4}$$

with the properties: $\|\boldsymbol{k}\|^2 = \left\|\boldsymbol{k}'\right\|^2 = -\|\boldsymbol{k}_3\|^2 = 1$. Here, $\boldsymbol{k}_2$ and $\boldsymbol{k}_3$ are the central normal and the asymptotic normal of $\mathfrak{M}$, respectively. The Blaschke

formula is:

$$
\begin{bmatrix} \boldsymbol{k}'_1 \\ \boldsymbol{k}'_2 \\ \boldsymbol{k}'_3 \end{bmatrix} = \begin{bmatrix} 0 & 1 & 0 \\ -1 & 0 & g \\ 0 & g & 0 \end{bmatrix} \begin{bmatrix} \boldsymbol{k}_1 \\ \boldsymbol{k}_2 \\ \boldsymbol{k}_3 \end{bmatrix} = \boldsymbol{\varrho} \times \begin{bmatrix} \boldsymbol{k}_1 \\ \boldsymbol{k}_2 \\ \boldsymbol{k}_3 \end{bmatrix}, \tag{5}
$$

where $\boldsymbol{\varrho}(v) = g(v)\boldsymbol{k_1}(v) - \boldsymbol{k_3}(v)$ is the Darboux vector. In this paper, we assume $\boldsymbol{z}(v)$ to be a $\mathfrak{TL}$-curve. Thus,

$$
\boldsymbol{z}(v) = \int\limits_0^v (\lambda(v)\boldsymbol{k}_1(v) + \mu(v)\boldsymbol{k}_3(v))dv, \text{ with } |\mu| > |\lambda|. \tag{6}
$$

Therefore, the $\mathfrak{TL}$-ruled surface is:

$$
\mathfrak{M} : \boldsymbol{x}(v,t) = \boldsymbol{z}(v) + t\boldsymbol{k}_1(v), \ t \in I, \ v \in \mathbb{R}. \tag{7}
$$

Here, $g(v)$, $\mu(v)$ and $\lambda(v)$ are the Blaschke invariants of $\boldsymbol{k}(v) \in \mathcal{S}_1^2$. Specifically, $g(v)$ is the spherical curvature of $\boldsymbol{k}(v) \in \mathcal{S}_1^2$, $\lambda(v)$ represents the angle between $\boldsymbol{z}'$ and $\boldsymbol{k}_1$, and $\mu(v)$ is the distribution parameter of $\mathfrak{M}$. The $\mathfrak{GL}$-unit normal vector is given by

$$
\boldsymbol{e}(v,t) = \frac{\boldsymbol{x}_t \times \boldsymbol{x}_v}{\|\boldsymbol{x}_t \times \boldsymbol{x}_v\|} = \frac{\mu\boldsymbol{k}_2 + t\boldsymbol{k}_3}{\sqrt{\mu^2 - t^2}}, \text{ with } |\mu| > |t|, \tag{8}
$$

which is the central normal $\boldsymbol{k}_2$ at $\boldsymbol{z}(v)$ when $t = 0$. The $\mathfrak{TL}$-curvature-axis of $\boldsymbol{k}(v) \in \mathcal{S}_1^2$ is

$$
\boldsymbol{a}(v) = \frac{\boldsymbol{\varrho}}{\|\boldsymbol{\varrho}\|} = \frac{g}{\sqrt{1-g^2}}\boldsymbol{k}_1 - \frac{1}{\sqrt{1-g^2}}\boldsymbol{k}_3, \text{ with } |g| < 1. \tag{9}
$$

Let γ be the radii of curvature among $\boldsymbol{k}_1$ and $\boldsymbol{a}$. Then,

$$
\boldsymbol{a}(v) = \sinh\gamma\boldsymbol{k}_1 - \cosh\gamma\boldsymbol{k}_3, \text{ with } \tanh\gamma = g(v). \tag{10}
$$

Corollary 1. The curvature $\kappa(v)$, the torsion $\tau(v)$, and $g(v)$ of $\boldsymbol{k}_1(v) \in \mathcal{S}_1^2$ are given by

$$
\kappa(v) = \sqrt{1-g^2} = \frac{1}{\cosh\gamma} = \frac{1}{\rho(v)}, \ \tau(v) := \pm\gamma' = \pm\frac{g'}{1-g^2}. \tag{11}
$$

Corollary 2. If $g(v) = const.$, then $\boldsymbol{k}_1(v) \in \mathcal{S}_1^2$ is a Lorentzian circle.
Proof. From Eq. (11), if $g = const.$, then $\tau(v) = 0$ and $\kappa(v) = const.$, which which implies that $\boldsymbol{k}_1(v) \in \mathcal{S}_1^2$ is a Lorentzian circle ∎.

4

Darboux frame   The Darboux frame of a ruled surface provides a natural moving frame along the rulings, incorporating both the geometry of the base curve and the surface itself. For the skew $\mathfrak{TL}$-ruled surface $\mathfrak{M}$ the Darboux frame $\{z'; \ b_1, b_2, b_3\}$ is defined as follows:

- $b_1(v) = z'(v) \left\| z'(v) \right\|^{-1}$ is the $\mathfrak{TL}$-unit tangent to z,
- $b_3 = -k_2(v)$ is the $\mathfrak{SL}$-unit normal to the surface along $z(v)$,
- $b_2(v) = b_3 \times b_1$ the $\mathfrak{SL}$-unit tangent to the ruled surface $\mathfrak{M}$.

In view of the statement above, the Darboux frame $\{b_1, b_2, b_3\}$ along the striction curve $z(v)$ satisfies:

$$\begin{bmatrix} b_1 \\ b_2 \\ b_3 \end{bmatrix} = \begin{bmatrix} \frac{\lambda}{\sqrt{\mu^2 - \lambda^2}} & 0 & \frac{\mu}{\sqrt{\mu^2 - \lambda^2}} \\ \frac{\mu}{\sqrt{\mu^2 - \lambda^2}} & 0 & \frac{\lambda}{\sqrt{\mu^2 - \lambda^2}} \\ 0 & -1 & 0 \end{bmatrix} \begin{bmatrix} k_1 \\ k_2 \\ k_3 \end{bmatrix}. \tag{12}$$

By differentiating both sides of the previous equations, we obtain

$$\begin{bmatrix} b_1' \\ b_2' \\ b_3' \end{bmatrix} = \begin{bmatrix} 0 & a_g & a_n \\ a_g & 0 & \tau_g \\ a_n & -\tau_g & 0 \end{bmatrix} \begin{bmatrix} b_1 \\ b_2 \\ b_3 \end{bmatrix}, \tag{13}$$

where

$$a_g(v) = \frac{1}{\mu^2 - \lambda^2}(\mu\lambda' - \lambda\mu'), \ a_n(v) = \frac{\lambda + g\mu}{\mu^2 - \lambda^2}, \ \tau_g(v) = \frac{\mu + g\lambda}{\mu^2 - \lambda^2}. \tag{14}$$

Here, $a_g(v)$, $a_n(v)$, and $\tau_g(v)$ represent the geodesic curvature, normal curvature, and geodesic torsion of $z(v)$, respectively. These relations characterize the geometric behavior of the $\mathfrak{TL}$-ruled surface in terms of its intrinsic and extrinsic properties. Therefore, we obtain the following conditions:

1) $z(v)$ is a geodesic $\mathfrak{TL}$-curve if and only if $a_g(v) = 0$, which simplifies to $\mu\lambda' - \lambda\mu' = 0$.

2) $z(v)$ is an asymptotic $\mathfrak{TL}$-curve if and only if $a_n(v) = 0$, which simplifies to $\lambda + g\mu = 0$.

3) $z(v)$ is a $\mathfrak{TL}$-curvature line if and only if $\tau_g(v) = 0$, which simplifies to $\mu + g\lambda = 0$.

Remark 1. From Eq. (7) and the above definitions, the following cases arise:
(a) if $\mu(v) = 0$, then $\mathfrak{M}$ is a $\mathfrak{TL}$-tangential developable, leading to

$$a_g(v) = 0, \ a_n(v) = -\frac{1}{\lambda}, \ \tau_g(v) = -\frac{g}{\lambda},$$

(b) if $\lambda(v) = 0$, then $\mathfrak{M}$ corresponds to a $\mathfrak{TL}$-binormal surface, resulting in

$$a_g(v) = 0, \ a_n(v) = \frac{g}{\mu}, \ \tau_g(v) = \frac{1}{\mu},$$

(c) if both $\lambda(v) = 0$ and $\mu(v) = 0$, then $\mathfrak{M}$ is a $\mathfrak{TL}$-cone, which implies

$$a_g(v) = a_n(v) = \tau_g(v) = 0.$$

3.1 Height functions

Consistent with [28], a point $\boldsymbol{a}_0(v) \in \mathcal{S}_1^2$ serves as a j-curvature axis of $\boldsymbol{k}_1(v) \in \mathcal{S}_1^2$ if, for all v, the condition $< \boldsymbol{a}_0, \boldsymbol{k}_1^j(v) >= 0$ is satisfied, while $< \boldsymbol{a}_0, \boldsymbol{k}_1^{j+1}(v) >\neq 0$. Here $\boldsymbol{k}_1^{j+1}$ denotes the j+1-th derivative of $\boldsymbol{k}(v)$ with respect to v. For the first curvature-axis $\boldsymbol{a}$ of $\boldsymbol{k}_1(v)$, we obtain the relations

$$< \boldsymbol{a}, \boldsymbol{k}_1^{'} >= \pm < \boldsymbol{a}, \boldsymbol{k}_2 >= 0,$$

and

$$< \boldsymbol{a}, \boldsymbol{k}_1^{''} >= \pm < \boldsymbol{a}, -\boldsymbol{k}_1 + g\boldsymbol{k}_3 >\neq 0.$$

Thus, $\boldsymbol{a}$ is at least an $\boldsymbol{a}_2$ curvature-axis of $\boldsymbol{k}_1(v) \in \mathcal{S}_1^2$. Next, we introduce the function $\varrho : I \times \mathcal{S}_1^2 \to \mathbb{R}$, defined as

$$\varrho(v, \boldsymbol{a}_0) =< \boldsymbol{a}_0, \boldsymbol{k}_1 > .$$

For any given position $\boldsymbol{k}_1(v) \in \mathcal{S}_1^2$, we adopt the notation $\varrho(v) = \varrho(v, \boldsymbol{a}_0)$.

Proposition 1.

   Under the given assumptions:

i- The function ϱ belongs to the first assessment if and only if $\boldsymbol{a}_0 \in Sp\{\boldsymbol{k}_1, \boldsymbol{k}_3\}$, meaning

$$\varrho^{'} = 0 \Leftrightarrow < \boldsymbol{k}_1^{'}, \boldsymbol{a}_0 >= 0 \Leftrightarrow < \boldsymbol{k}_2, \boldsymbol{a}_0 >= 0 \Leftrightarrow \boldsymbol{a}_0 = c_1\boldsymbol{k}_1 + c_3\boldsymbol{k}_3;$$

where $c_1, c_3 \in \mathbb{R}$ satisfy the relation $c_1^2 - c_3^2 = 1$.

ii- ϱ is in the second assessment if and only if $\boldsymbol{a}_0$ is the $\boldsymbol{a}_2$ curvature-axis of $\boldsymbol{k}_1(v) \in \mathcal{S}_1^2$, meaning

$$\varrho^{'} = \varrho^{''} = 0 \Leftrightarrow \boldsymbol{a}_0 = \pm \boldsymbol{a}.$$

iii- ϱ belongs to the third assessment if and only if $\boldsymbol{a}_0$ is the $\boldsymbol{a}_3$ curvature-axis of $\boldsymbol{k}_1(v) \in \mathcal{S}_1^2$, meaning

$$\varrho^{'} = \varrho^{''} = \varrho^{'''} = 0 \Leftrightarrow \boldsymbol{a}_0 = \pm \boldsymbol{a}, \text{ and } g^{'} \neq 0.$$

iv- ϱ is classified under the fourth assessment if and only if $\boldsymbol{a}_0$ is the $\boldsymbol{a}_4$ curvature-axis of $\boldsymbol{k}_1(v) \in \mathcal{S}_1^2$, meaning

$$\varrho^{'} = \varrho^{''} = \varrho^{'''} = \varrho^{iv} = 0 \Leftrightarrow \boldsymbol{a}_0 = \pm \boldsymbol{a}, \ g^{'} = 0, \text{ and } g^{''} \neq 0.$$

Proof. For $\varrho^{'}$, we observe that:

$$\varrho^{'} =< \boldsymbol{k}_1^{'}, \boldsymbol{a}_0 >. \tag{15}$$

Thus,

$$\varrho^{'} = 0 \Leftrightarrow < \boldsymbol{k}_2, \boldsymbol{a}_0 >= 0 \Leftrightarrow \boldsymbol{a}_0 = c_1\boldsymbol{k}_1 + c_3\boldsymbol{k}_3; \tag{16}$$

where $c_1, c_3 \in \mathbb{R}$ and satisfy $c_1^2 - c_3^2 = 1$, the conclusion follows immediately.

2- Differentiating Eq. (15), we obtain:

$$\varrho^{''} =< \boldsymbol{k}_1^{''}, \boldsymbol{a}_0 >= < -\boldsymbol{k}_1 + g\boldsymbol{k}_3, \boldsymbol{a}_0 > . \tag{17}$$

From Eqs. (16) and (17), we deduce

$$\varrho' = \varrho'' = 0 \Leftrightarrow < k_1', a_0 > = < k_1'', a_0 > = 0 \Leftrightarrow a_0 = \pm \frac{k_1' \times k_1''}{\left\| k_1' \times k_1'' \right\|} = \pm a.$$

3- Differentiating Eq. (17), we find:

$$\varrho''' = < k_1''', a_0 > = \left(-1 + g^2\right) < k_2, a_0 > + g' < k_3, a_0 >$$

Thus, we obtain

$$\varrho' = \varrho'' = \varrho''' = 0 \Leftrightarrow a_0 = \pm a, \text{ and } g' \neq 0.$$

4- By applying the same differentiation process, we also find

$$\varrho' = \varrho'' = \varrho''' = \varrho^{iv} = 0 \Leftrightarrow a_0 = \pm a, \, g' = 0, \text{ and } g'' \neq 0.$$

This completes the proof. ∎

Consequences of Proposition 1:
(a) The osculating circle $\mathcal{S}(\rho, a_0)$ of $k_1(v) \in \mathcal{S}_1^2$ satisfies

$$< a_0, k_1 > = \sinh \gamma, \; < k_1', a_0 > = 0, < k_1'', a_0 > = 0.$$

This condition ensures that the osculating circle has at least third-order contact with $k_1(v_0)$ if and only if $g' \neq 0$.
(b) The curve $k_1(v) \in \mathcal{S}_1^2$ and the osculating circle $\mathcal{S}(\rho, a_0)$ attain at least fourth-order contact at $k_1(v_0)$ if and only if $g' = 0$ and $g'' \neq 0$.
    Following this approach, by considering the curvature axes $k_1(v) \in \mathcal{S}_1^2$, we can establish a sequence of curvature axes: a_2, a_3,..., a_n. The properties and interconnections among these curvature centers present intriguing challenges. For instance, it is straightforward to observe that if $a_0 = \pm a$, and $g' = 0$, then $k_1(v)$ is positioned at a fixed γ relative to a_0. In this case, the curvature axis remains well-defined up to the second order, and $\mathfrak{M}$ is a slant $\mathfrak{TL}$-ruled surface.

Theorem 1. A surface $\mathfrak{M}$ is a slant $\mathfrak{TL}$-ruled surface if and only if $g(v) = const.$

Definition 1. Let $\mathfrak{M}$ and $\mathfrak{M}^*$ be two skew $\mathfrak{TL}$-ruled surfaces in $\mathbb{E}_1^3$. The surface $\mathfrak{M}^*$ is termed an evolute offset of $\mathfrak{M}$ if there exists a one-to-one correspondence between their rulings such that the central normal of $\mathfrak{M}$ aligns coaxially with the ruling direction of $\mathfrak{M}^*$.

Assume $\mathfrak{M}^*$ is an evolute offset of $\mathfrak{M}$ and and let its associated Blaschke frame be given by $\{z^*(v^*); k_1^*(v^*), k_2^*(v^*), k_3^*(v^*)\}$ as formulated in Eqs. (5)-(7). Then, the parametric representation of $\mathfrak{M}^*$ is

$$\mathfrak{M}^* : x^*(v^*, t) = z^*(v^*) + t k_1^*(v^*), \; t \in \mathbb{R}, \tag{18}$$

where
$$\boldsymbol{z}^*(v^*) = \boldsymbol{z}(v) + \gamma^*(v)\boldsymbol{k}_2(v), \tag{19}$$

and $\gamma^*(v) = \|\boldsymbol{z}^*(v^*) - \boldsymbol{z}(v)\|$ represents the Lorentzian norm. Given that $\boldsymbol{k}_1^* = \boldsymbol{k}_2$ at striction points, it follows that

$$\boldsymbol{k}_2^* := \frac{\boldsymbol{k}_2'}{\left\|\boldsymbol{k}_2'\right\|} = \frac{-1}{\sqrt{1-g^2}}\boldsymbol{k}_1 + \frac{g}{\sqrt{1-g^2}}\boldsymbol{k}_3, \tag{20}$$

and

$$\boldsymbol{k}_3^* := \boldsymbol{k}_1^* \times \boldsymbol{k}_2^* = -\frac{g}{\sqrt{1-g^2}}\boldsymbol{k}_1 + \frac{1}{\sqrt{1-g^2}}\boldsymbol{k}_3. \tag{21}$$

Since $\boldsymbol{k}_1^* = \boldsymbol{k}_2$, from Eqs. (20) and (21), we obtain:

$$\begin{bmatrix} \boldsymbol{k}_1^* \\ \boldsymbol{k}_2^* \\ \boldsymbol{k}_3^* \end{bmatrix} = \begin{bmatrix} 0 & 1 & 0 \\ -\cosh\gamma & 0 & \sinh\gamma \\ -\sinh\gamma & 0 & \cosh\gamma \end{bmatrix} \begin{bmatrix} \boldsymbol{k}_1 \\ \boldsymbol{k}_2 \\ \boldsymbol{k}_3 \end{bmatrix}. \tag{22}$$

If v^* denotes the arc-length parameter of $\boldsymbol{k}_1^* \in \mathcal{S}_1^2$, then $dv^* := \left\|\boldsymbol{k}_2'\right\| dv = \sqrt{1-g^2}dv$. Consequently,

$$\frac{d}{dv^*} \begin{bmatrix} \boldsymbol{k}_1^* \\ \boldsymbol{k}_2^* \\ \boldsymbol{k}_3^* \end{bmatrix} = \begin{bmatrix} 0 & 1 & 0 \\ -1 & 0 & g^* \\ 0 & g^* & 0 \end{bmatrix} \begin{bmatrix} \boldsymbol{k}_1^* \\ \boldsymbol{k}_2^* \\ \boldsymbol{k}_3^* \end{bmatrix}, \tag{23}$$

where

$$g^*(v) = \frac{g'(v)}{(1-g^2(v))^{\frac{3}{2}}}. \tag{24}$$

Corollary 3. If $g(v)$ remains constant, then $\boldsymbol{k}_1^*(v^*)$ describes a Lorentzian small circle on $\mathcal{S}_1^2$.

3.2 Construction of $\mathfrak{M}$ and $\mathfrak{M}^*$

Given that $g(v)$ is a constant, we derive from Eqs. (5) and (11) the following ordinary differential equation: $\boldsymbol{k}_1''' + \kappa^2 \boldsymbol{k}_1' = \boldsymbol{0}$. It is convenient to introduce $d\phi = \kappa dv$. Moreover, by setting $\boldsymbol{k}_1'(0) = (0,1,0)$, we obtain

$$\boldsymbol{k}_1(\phi) = (\cosh\gamma\cos\phi, \cosh\gamma\sin\phi, \sinh\gamma), \tag{25}$$

where $0 \leq \varphi \leq 2\pi$. Consequently, we determine

$$\left. \begin{aligned} \boldsymbol{k}_2(\phi) &= \frac{d\boldsymbol{k}_1}{d\phi}\left\|\frac{d\boldsymbol{k}_1}{d\phi}\right\|^{-1} = (-\sin\phi, \cos\phi, 0), \\ \boldsymbol{k}_3(\phi) &= \boldsymbol{k}_1 \times \boldsymbol{k}_2 = (-\sinh\gamma\cos\phi, -\sinh\gamma\sin\phi, -\cosh\gamma). \end{aligned} \right\} \tag{26}$$

8

By applying Eqs. (6) and (7), the position vector $\boldsymbol{z}(\phi)$ is formulated as

$$
\boldsymbol{z}(\phi) := \begin{bmatrix} z_1 \\ z_2 \\ z_3 \end{bmatrix} = \begin{bmatrix} (\int\limits_0^\phi \lambda \cos\phi d\phi)\cosh\gamma - (\int\limits_0^\phi \mu \cos\phi d\phi)\sinh\gamma \\ (\int\limits_0^\phi \lambda \sin\phi d\phi)\cosh\gamma - (\int\limits_0^\phi \mu \sin\phi d\phi)\sinh\gamma \\ (\int\limits_0^\phi \lambda d\phi)\sinh\gamma - (\int\limits_0^\phi \mu d\phi)\cosh\gamma \end{bmatrix} \tag{27}
$$

From Eqs. (7) and (28), we define the $\mathfrak{TL}$-ruled surface $\mathfrak{M}$ as

$$
\mathfrak{M} : \boldsymbol{x}(\phi, t) = (z_1, z_2, z_3) + t \left(\cosh\gamma \sin\phi, \cosh\gamma \cos\phi, \sinh\gamma \right). \tag{28}
$$

Similarly, employing Eqs. (18), (19), and (28), the evolute offset surface $\mathfrak{M}^*$ takes the form

$$
\mathfrak{M}^* : \boldsymbol{x}^*(\phi, t) = (z_1 + (\gamma^* - t)\sin\phi, z_2 + (\gamma^* + t)\cos\phi, z_3). \tag{29}
$$

3.2.1 Classification of $\mathfrak{M}$ and $\mathfrak{M}^*$

To proceed with classification, we assign $\gamma = 1.5$, and $\gamma^*(\phi) = \sinh\phi$. Utilizing Eqs. (28) and (29) alongside various selections for $\mu(\phi)$, and $\lambda(\phi)$, we can categorize the pair $(\mathfrak{M}, \mathfrak{M}^*)$ accordingly.

1). Let $\boldsymbol{z}(\phi)$ represent an asymptotic $\mathfrak{TL}$-curve, meaning that the normal curvature satisfies $a_n(v) = 0$, which leads to the condition $\lambda + g\mu = 0$. The corresponding $\mathfrak{TL}$-ruled surface pair $(\mathfrak{M}, \mathfrak{M}^*)$ is depicted in Figure 1, with $\mu(\phi) = \phi$, $0 \le \phi \le 2\pi$ and $-10 \le t \le 10$.

Figure 1. $\mathfrak{M}$ (left) and its evolute offset $\mathfrak{M}^*$ (right).

2). Consider $z(\phi)$ as a geodesic $\mathfrak{TL}$-curve, which implies that the geodesic curvature satisfies $a_g(v) = 0$. This condition results in the equation $\mu\lambda' - \lambda\mu' = 0$. The associated $\mathfrak{TL}$-ruled surface pair $(\mathfrak{M}, \mathfrak{M}^*)$ is illustrated in Figure 2, where $\lambda(\phi) = \mu(\phi) = \phi$, $0 \leq \phi \leq 2\pi$ and $-0.5 \leq t \leq 0.5$.

Figure 2. $\mathfrak{M}$ (left) and its evolute offset $\mathfrak{M}^*$ (right).

3). Let $z(\phi)$ be a $\mathfrak{TL}$-curvature line, meaning that the geodesic torsion satisfies $\tau_g(v) = 0$. This condition leads to the equation $\mu + \lambda g = 0$. The corresponding $\mathfrak{TL}$-ruled surface pair $(\mathfrak{M}, \mathfrak{M}^*)$ is depicted in Figure 3, where $\mu(\phi) = \phi$, $0 \leq \phi \leq 2\pi$ and $-5 \leq t \leq 5$.

Figure 3. $\mathfrak{M}$ (left) and its evolute offset $\mathfrak{M}^*$ (right).

10

4) Consider the case where $\mu(\phi) = 0$, implying that $\mathfrak{M}$ is a $\mathfrak{TL}$-developable surface. The associated $\mathfrak{TL}$-ruled surface pair $(\mathfrak{M}, \mathfrak{M}^*)$ is illustrated in Figure 3, where $\lambda(\phi) = \varphi$, $0 \leq \phi \leq 2\pi$ and $-5 \leq t \leq 5$.

Figure 4. $\mathfrak{M}$ (left) and its evolute offset $\mathfrak{M}^*$ (right).

5) If $\lambda(\phi) = 0$, then $\mathfrak{M}$ represents a $\mathfrak{TL}$-binormal surface. The corresponding $\mathfrak{TL}$-ruled surface pair is depicted in Figure 5, with $\mu(\phi) = \phi$, $0 \leq \phi \leq 2\pi$ and $-5 \leq t \leq 5$.

Figure 5. $\mathfrak{M}$ (left) and its evolute offset $\mathfrak{M}^*$ (right).

6) When $\lambda(\phi) = \mu(\phi) = 0$, the surface $\mathfrak{M}$ is classified as a $\mathfrak{TL}$-cone. The corresponding ruled surface pair $(\mathfrak{M}, \mathfrak{M}^*)$ is illustrated in Figure 6, where $0 \leq$

$\varphi \leq 2\pi$ and $-5 \leq t \leq 5$.

Figure 6. $\mathfrak{M}$ (left) and its evolute offset $\mathfrak{M}^*$ (right)

4   Conclusion

This study examined the fundamental properties of slant $\mathfrak{TL}$-ruled surfaces and their evolute offsets in Minkowski space $\mathbb{E}_1^3$. By establishing a direct relationship between the central normal of $\mathfrak{M}$ and the ruling of $\mathfrak{M}^*$, we formulated essential conditions governing their geometric structure. Through analytical derivations, we classified these surfaces based on curvature properties and special parameter choices, highlighting cases such as $\mathfrak{TL}$-developable and $\mathfrak{TL}$-binormal surfaces. The graphical representations further illustrated these classifications, providing insight into their structural behavior. These findings contribute to the broader study of ruled surfaces in Lorentzian geometry, with potential applications in mathematical physics and related fields. In the recipient work, we blueprint to go forward to look the categorization of singularities as they are sharped in [25, 26].

4.1   Use of AI tools declaration

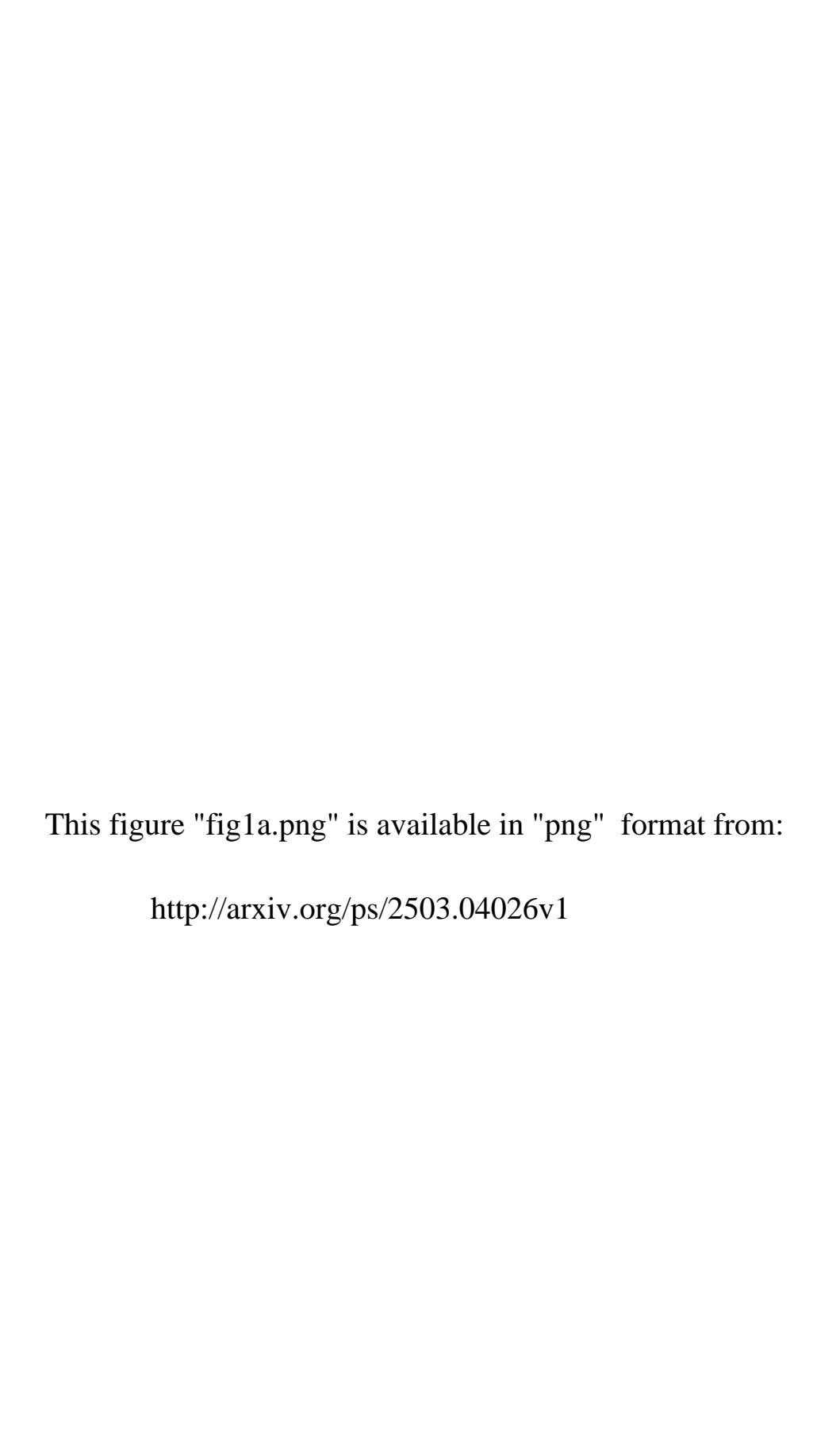The authors declare that they have not used artificial intelligence tools in the creation of this article.
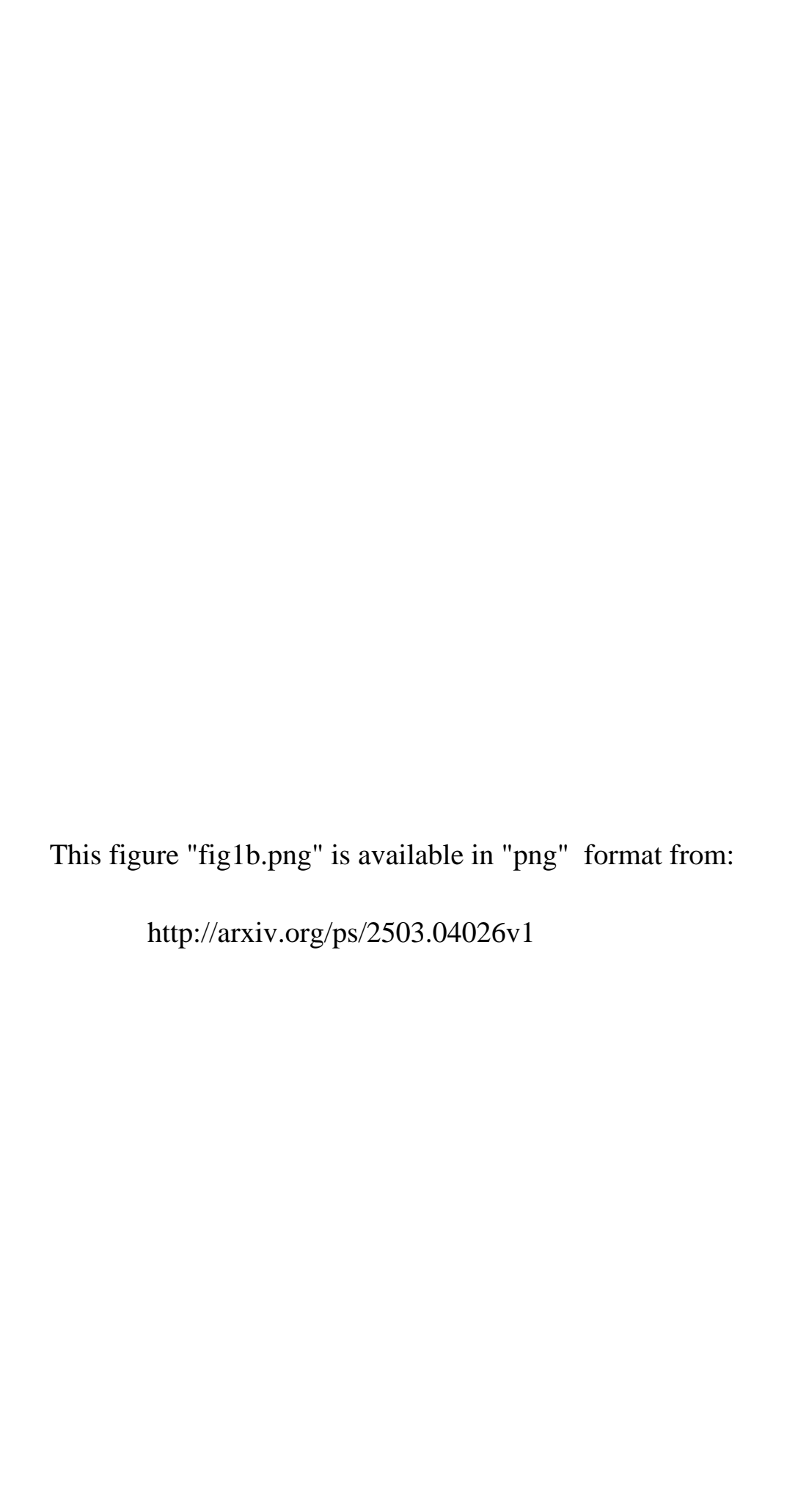
4.2   Conflict of interest

The authors advertise that they have no conflict.

References

[1] H.W. Gugenheimer. Differential Geometry, Graw-Hill, New York, pp.162-169,(1956).

[2] O. Bottema & B. Roth. Theoretical Kinematics, North-Holland Press, New York, (1979).

[3] A. Karger & J. Novak. Space Kinematics and Lie Groups, Gordon and Breach Science Publishers, New York, (1985).

[4] S.G. Papaionnou & D. Kiritsis. An application of Bertrand curves and surfaces to CAD/CAM, Computer Aided Design 17 (8) (1985) 348-352.

[5] J.A. Schaaf. Geometric Continuity of Ruled Surfaces, Computer Aided Geometric Design 15, pp.289-310, (1998).

[6] M. Peternell & H. Pottmann, B. Ravani. On the computational geometry of ruled surfaces, Comput.-Aided Design 31 (1999) 17–32.

[7] H. Pottman & J. Wallner. Computational Line Geometry, Springer-Verlag, Berlin, Heidelberg, (2001).

[8] B. Ravani & T.S. Ku. Bertrand offsets of ruled and developable surfaces, Computer Aided design, 23 (2), (1991) 145-152.

[9] A. Küçük & O. Gürsoy. On the invariants of Bertrand trajectory surface offsets, AMC, (2003) 11-23.

[10] E. Kasap & N. Kuruoglu. Integral invariants of the pairs of the Bertrand ruled surface, Bull. Pure Appl. Sci. Sect. E Math., 21(2002), 37-44.

[11] E. Kasap & N. Kuruoglu. The Bertrand offsets of ruled surfaces in R_1^3, Acta Math Vietnam 2006; 31: 39-48.

[12] E. Kasap, S. Yuce & N. Kuruoglu. The involute-evolute offsets of ruled surfaces. Iranian J Sci Tech Transaction A 2009; 33: 195-201.

[13] K. Orbay, E. Kasap & I. Aydemir. Mannheim offsets of ruled surfaces, Math Problems Engineering, (2009), Article Id 160917.

[14] M. Onder & H.H Ugurlu. Frenet frames and invariants of timelike ruled surfaces. Ain Shams Eng. J 2013; 4: 507-513.

[15] G.Y. Sentrk & S. Yuce. Properties of integral invariants of the involute-evolute offsets of ruled surfaces, Int. J. Pure Appl. Math., 102(2015), 757-768.

[16] D.W. Yoon. On the evolute offsets of ruled surfaces in Euclidean 3-space, Inter. J. of Pure and App. Maths. V. 108 No. 4 2016, 985-997.

[17] D.W. Yoon. On the evolute offsets of ruled surfaces in Minkowski 3-space, Turk. J. Math., (2016) 40: 594 – 604.

[18] M.T. Aldossary& R.A. Abdel-Baky. On the Blaschke approach of Bertrand offsets of spacelike ruled surfaces, AIMS Mathematics, 2022, Volume 6, Issue 4: 3339-3351.

[19] N. Alluhaibi, R.A. Abdel-Baky & M. Naghi. On the Bertrand Offsets of Timelike Ruled Surfaces in Minkowski 3-Space. Symmetry, 2022, .No. 4, p. 673.

[20] S. Nazra & R A. Abdel-Baky. Bertrand offsets of ruled surfaces with Blaschke frame in Euclidean 3-space. Axioms 2023, 12, 649.

[21] F. Mofarreh & R.A. Abdel-Baky. Surface pencil pair interpolating Bertrand pair as common asymptotic curves in Euclidean 3-space. Mathematics 11.16 (2023): 3495.

[22] J. Walfare. Curves and Surfaces in Minkowski Space. Ph.D. Thesis, K.U. Leuven, Faculty of Science, Leuven, Belgium, 1995.

[23] B. O'Neil. Semi-Riemannian Geometry Geometry, with Applications to Relativity; Academic Press: New York, NY, USA, 1983.

[24] JW. Bruce & PJ. Giblin. Generic geometry, the American Mathematical Monthly, Vol. 90, No. 8, pp. 529–545, 1983.

[25] A. Almoneef & R.A. Abdel-Baky. Singularity properties of spacelike circular surfaces, Symmetry 2023, 15, 842.

[26] S. Nazra & R A. Abdel-Baky. Singularities of non-lightlike developable surfaces in Minkowski 3-space, Mediterr. J. Math. (2023) 20:45.

This figure "fig1a.png" is available in "png" format from:

http://arxiv.org/ps/2503.04026v1

This figure "fig1b.png" is available in "png" format from:

http://arxiv.org/ps/2503.04026v1

This figure "fig2a.png" is available in "png" format from:

http://arxiv.org/ps/2503.04026v1

This figure "fig2b.png" is available in "png" format from:

http://arxiv.org/ps/2503.04026v1

This figure "fig3a.png" is available in "png" format from:
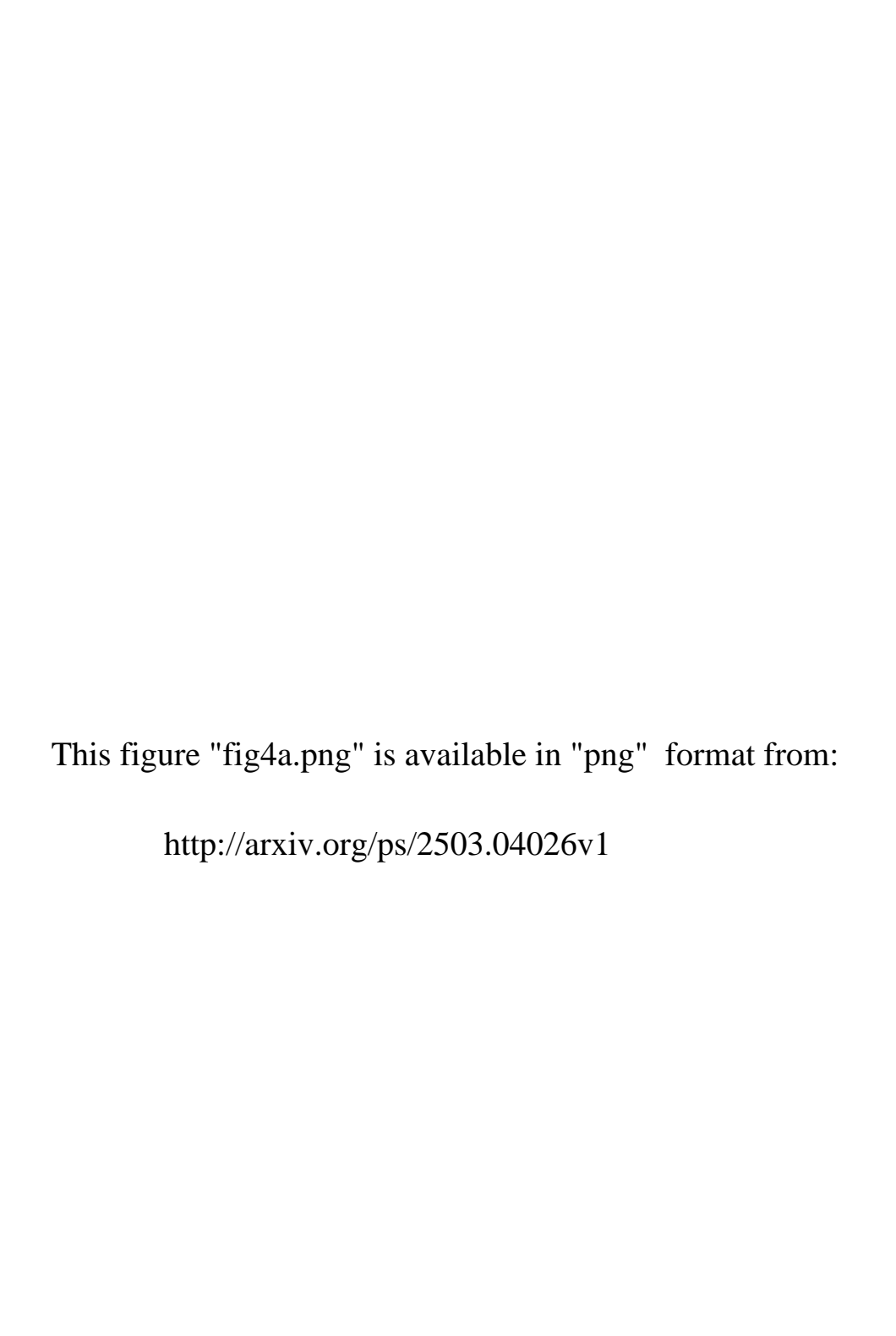
http://arxiv.org/ps/2503.04026v1

This figure "fig3b.png" is available in "png" format from:

http://arxiv.org/ps/2503.04026v1

This figure "fig4a.png" is available in "png" format from:

http://arxiv.org/ps/2503.04026v1
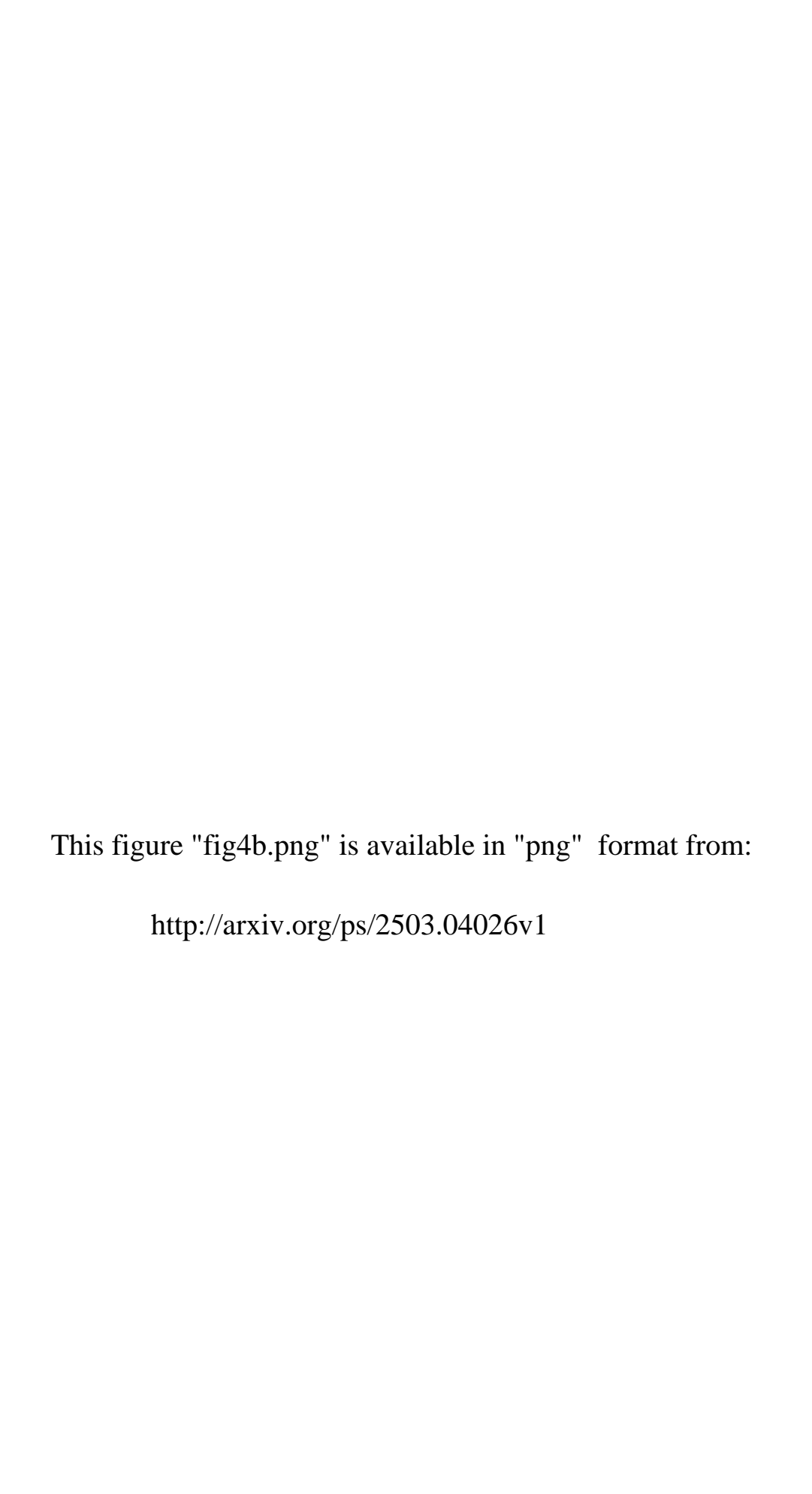
This figure "fig4b.png" is available in "png" format from:

http://arxiv.org/ps/2503.04026v1

This figure "fig5a.png" is available in "png" format from:

http://arxiv.org/ps/2503.04026v1

This figure "fig5b.png" is available in "png" format from:

http://arxiv.org/ps/2503.04026v1

This figure "fig6a.png" is available in "png" format from:

http://arxiv.org/ps/2503.04026v1

This figure "fig6b.png" is available in "png" format from:

http://arxiv.org/ps/2503.04026v1